

University of Wollongong
Research Online

Faculty of Engineering and Information
Sciences - Papers: Part A

Faculty of Engineering and Information
Sciences

1-1-2013

Catalytic role of ge in highly reversible GeO₂/Ge/C nanocomposite anode material for lithium batteries

Kuok Hau Seng
University of Wollongong, kseng@uow.edu.au


Mi-Hee Park
Ulsan National Institute of Science and Technology

Zai Ping Guo
University of Wollongong, zguo@uow.edu.au

Hua-Kun Liu
University of Wollongong, hua@uow.edu.au

Jaephil Cho
Ulsan National Institute of Science and Technology

Follow this and additional works at: <https://ro.uow.edu.au/eispapers>

 Part of the [Engineering Commons](#), and the [Science and Technology Studies Commons](#)

Recommended Citation

Seng, Kuok Hau; Park, Mi-Hee; Guo, Zai Ping; Liu, Hua-Kun; and Cho, Jaephil, "Catalytic role of ge in highly reversible GeO₂/Ge/C nanocomposite anode material for lithium batteries" (2013). *Faculty of Engineering and Information Sciences - Papers: Part A*. 552.
<https://ro.uow.edu.au/eispapers/552>

Research Online is the open access institutional repository for the University of Wollongong. For further information contact the UOW Library: research-pubs@uow.edu.au

Catalytic role of ge in highly reversible GeO₂/Ge/C nanocomposite anode material for lithium batteries

Abstract

GeO₂/Ge/C anode material synthesized using a simple method involving simultaneous carbon coating and reduction by acetylene gas is composed of nanosized GeO₂/Ge particles coated by a thin layer of carbon, which is also interconnected between neighboring particles to form clusters of up to 30 μm. The GeO₂/Ge/C composite shows a high capacity of up to 1860 mAh/g and 1680 mAh/g at 1 C (2.1 A/g) and 10 C rates, respectively. This good electrochemical performance is related to the fact that the elemental germanium nanoparticles present in the composite increases the reversibility of the conversion reaction of GeO₂. These factors have been found through investigating and comparing GeO₂/Ge/C, GeO₂/C, nanosized GeO₂, and bulk GeO₂. © 2013 American Chemical Society.

Keywords

geo₂, reversible, batteries, highly, lithium, ge, role, catalytic, material, anode, nanocomposite, c

Disciplines

Engineering | Science and Technology Studies

Publication Details

Seng, K. Hau., Park, M., Guo, Z. Ping., Liu, H. Kun. & Cho, J. (2013). Catalytic role of ge in highly reversible GeO₂/Ge/C nanocomposite anode material for lithium batteries. *Nano Letters: a journal dedicated to nanoscience and nanotechnology*, 13 (3), 1230-1236.

Catalytic Role of Ge in Highly Reversible GeO₂/Ge/C Nanocomposite Anode Material for Lithium Batteries

Kuok Hau Seng,^{†§} Mi-hee Park,^{‡§} Zai Ping Guo,^{†} Hua Kun Liu,[†] and Jaephil Cho^{‡*}*

[†]Institute for Superconducting and Electronic Materials (ISEM), University of Wollongong, 2522
NSW, Australia

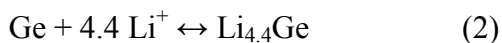
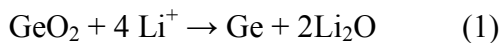
[‡]Interdisciplinary School of Green Energy, Ulsan National Institute of Science and Technology
(UNIST), Ulsan 689-798, South Korea

Abstract: GeO₂/Ge/C anode material synthesized using a simple method involving simultaneous carbon coating and reduction by acetylene gas is composed of nanosized GeO₂/Ge particles coated by a thin layer of carbon, which is also interconnected between neighboring particles to form clusters of up to 30 micrometers. The GeO₂/Ge/C composite shows high capacity of up to 1860 mAh/g and 1680 mAh/g at 1C (2.1 A/g) and 10C rates, respectively. This good electrochemical performance is related to the fact that the elemental germanium nanoparticles present in the composite increases the reversibility of the conversion reaction of GeO₂. These factors have been found through investigating and comparing GeO₂/Ge/C, GeO₂/C, nanosized GeO₂, and bulk GeO₂.

Keywords: germanium dioxide, high capacity, anode, lithium batteries

Graphite has been used as the commercial anode material since the introduction of LIBs in the 1990s, although it has a quite low theoretical capacity of 372 mAh/g. Thus, much research has been focused on high capacity materials such as silicon (4200 mAh/g),¹⁻⁶ germanium (1623 mAh/g),⁷⁻¹³ and tin (993 mAh/g)¹⁴⁻¹⁹ to replace the graphite anode. The oxides of these metals (SiO,²⁰⁻²³ GeO₂,²⁴⁻²⁸ SnO,^{29, 30} SnO₂³¹⁻³⁴) are another group of materials which can provide high lithium storage capacity. In addition, there is widespread belief that during the first lithiation, Li₂O is irreversibly formed. If the Li₂O component could be reversibly formed during cycling, these oxide materials could theoretically store up to 8.4 Li⁺. This would make them attractive alternatives as high capacity anode materials.

Germanium dioxide nanoparticles have been previously studied as anode material for LIBs and were reported to react with up to 9 Li⁺ during the first discharge cycle.²⁶ The lithium storage mechanism is described by an initial conversion reaction (Equation 1) followed by an alloying reaction (Equation 2). The lithium-ions, however, could not be fully removed in the subsequent charging cycle due to the irreversible Li₂O formation. This limits the theoretical lithium storage to 4.4 Li⁺ per GeO₂ (1126 mAh/g) compared to 8.4 Li⁺ (2152 mAh/g).



Recently, Kim *et al.* published a report on MGeO₃ (M = Cu, Fe, and Co), in which the reversible formation of Ge-O bonds during lithium insertion and extraction was studied using X-ray absorption spectroscopy.²⁸ One of the key factors contributing to the re-oxidation of metallic germanium during de-lithiation is the presence of the transition metal nanoparticles. The metallic nanoparticles play a catalytic role in the decomposition of Li₂O, and also form a conductive network between germanium and Li₂O to facilitate the re-oxidation of germanium. In addition,

an amorphous GeO_x ($x = 0.67$) hierarchical structure was also reported recently that showed a reversible conversion reaction.²⁴ As the GeO_x contains Ge-Ge and Ge-O bonds, with distances that are similar to the crystalline products, it is possible that the extra germanium in the structure plays a similar role as to that of the metallic copper in the work reported by Kim *et al.* In this work, catalyst role of Ge in $\text{GeO}_2/\text{Ge}/\text{C}$ nanocomposite anode is investigated using partially reduction of the GeO_2 in conjunction with the carbon coating process. The anode shows higher capacity and better rate capability than GeO_2/C nanocomposite.

A brief summary of the synthesis procedure is presented in Figure 1. The synthesis of GeO_2 nanoparticles through a simple hydrolysis method was reported in our previous work.¹³ Hereafter, the as-prepared GeO_2 nanoparticles will be referred to as “ GeO_2 -nano”. The GeO_2 -nano was heated to 520°C in acetylene/argon atmosphere for 30 minutes to form a uniform carbon coating layer on each of the particles, and the resultant sample is denoted as “ GeO_2/C ”. When the reaction temperature was increased to 650°C , partial reduction of the GeO_2 occurs in conjunction with the carbon coating process. The resultant sample from this process is denoted as “ $\text{GeO}_2/\text{Ge}/\text{C}$ ”. Reduction of the GeO_2 occurs due to the higher temperature ($> 600^\circ\text{C}$) and the reducing species formed by the decomposition of acetylene.^{4,13} Acetylene gas was chosen as the carbon source because of its ability to simultaneously granulate the nanoparticles into large micrometer sized clusters and form a uniform carbon coating layer. In addition, this method is known to be able to preserve the surface area of the precursor.⁴ From the Brunauer-Emmett-Teller (BET) analysis (Figure S1), GeO_2 -nano has a BET surface area of $109 \text{ m}^2/\text{g}$, and after carbon coating, GeO_2/C has a BET surface area of $101 \text{ m}^2/\text{g}$, which is a negligible reduction. However, the $\text{GeO}_2/\text{Ge}/\text{C}$ shows a lower BET surface area of $79 \text{ m}^2/\text{g}$, which is due to the reduction of GeO_2 to metallic germanium. In addition, the carbon coated samples were

characterized in an Elemental Analyzer (CHNS) to determine the amount of carbon present in the sample. The GeO₂/C and GeO₂/Ge/C have 11 wt% and 23 wt% carbon, respectively. The GeO₂/Ge/C has a higher content of carbon due to the higher reaction temperature and the lower mass after reduction of GeO₂.

Figure 2 shows the X-ray diffraction patterns (XRD; Rigaku SA-HFM3) of the as-synthesized GeO₂-nano, GeO₂/C, and GeO₂/Ge/C. Micrometer sized GeO₂ (Sigma Aldrich) was also characterized as a reference and control for the experiments. Hereafter, the micron-sized GeO₂ will be referred to as “GeO₂-bulk”. The XRD patterns of all the samples can be related to hexagonal phase (ICDD# 36-1463) GeO₂. It should be noted that the peaks of the GeO₂-nano sample appear very broad compared to GeO₂-bulk. This is due to the amorphous and nanocrystalline nature of the material. After carbon coating at higher temperature, the peaks in the GeO₂/C pattern remained similar to the pattern of GeO₂-nano. This confirms that no reduction of GeO₂ occurs at 520°C. As for the two peaks marked with an asterisk in the XRD pattern of GeO₂/Ge/C, they can be related to the diamond cubic phase (ICDD#04-0545) of germanium. This confirms the presence of two crystalline phases, hexagonal GeO₂ and diamond cubic Ge, in the sample. In order to determine the ratio of GeO₂ to Ge in the GeO₂/Ge/C sample, Rietveld refinement was performed, and the results are presented in Figure S2. The ratio of Ge to GeO₂ in the sample was determined to be 17:83. The weight fractions of the components in the composite are 64 wt% GeO₂, 13 wt% Ge, and 23 wt% C.

Morphologies of the samples were investigated using transmission electron microscope (TEM) as shown in Figure 3 (For SEM images of the samples, see SI; FigureS3). The GeO₂-nano sample (Figure 3a) has particles about 10 nm in size (dense area), and they are further covered by an amorphous layer (lighter area), which is due to the low temperature synthesis of the GeO₂-

nano sample. This is consistent with the broad peaks shown in the XRD pattern. After carbon coating, the amorphous layer is not observed, and this is due to the high temperature process, which increases the crystallinity (Figure 3b). When investigated using high resolution TEM (HRTEM), the average particle size of GeO₂/C was determined to be about 20 nm. Surprisingly, the carbon layer and the lattice spacing of GeO₂ could not be resolved (Figure 3c). This is due to the deformation of the particles when focused under the electron beam.³⁵ Figure 3d presents a typical TEM image of GeO₂/Ge/C where the morphology of the particles appears similar to that of GeO₂/C (Figure 4b). When investigated under HRTEM, the carbon coating layer clearly covers the nanoparticles, as marked by the black arrows in Figure 3e. Another interesting point to note is the inter-connected carbon shell between neighboring particles. This is an important factor, as the interconnected carbon shell network provides an efficient electronic route, which has been reported in our previous work.¹³ The insets of Figure 3f show an enlarged image of the area indicated by the white arrow and the corresponding Fast Fourier Transform (FFT) diffraction pattern. The *d*-spacing was measured to be 0.32 nm, which corresponds to the spacing of the (111) planes of cubic germanium. Similar to the GeO₂/C sample, no lattice spacing of GeO₂ can be observed, which is due to the electron beam induced deformation.

Lithium storage performances of the samples were tested in a coin type half-cell. In order to study the conversion reaction, a wide potential window of 0.01 V to 3.0 V was used for all the tests. The cycling performances of all samples are plotted in Figure 4a, and the corresponding first cycle voltage profiles are plotted in Figure 4b. For the first cycle, all the cells were discharged and charged at the 0.05 C-rate (1 C = 2.1 A/g = 1.05 mA/cm²), and in subsequent cycles the discharge was set to the 0.5 C-rate and the charge to the 1 C-rate. At the first cycle, the GeO₂-bulk exhibits discharge and charge capacities of 1587 mAh/g and 511 mAh/g,

respectively, corresponding to coulombic efficiency of 32%. Even though the GeO₂-bulk sample shows very low capacity, the capacity retention at higher rates is excellent. The charge capacity at the 1 C-rate remains 360 mAh/g over 50 cycles with negligible fading. Furthermore, the coulombic efficiencies of more than 99% after the first cycle agree with the stable cycling performance (Figure S4a). Nano-sized particles, on the other hand, show enhanced capacity due to the larger surface area and shorter lithium reaction pathways, which is evident from the GeO₂-nano sample. The first discharge and charge capacity of GeO₂-nano at the 0.05 C-rate is 2444 mAh/g and 1348 mAh/g, respectively, and the coulombic efficiency is 55%. The first discharge cycle shows reaction of 9.5 Li⁺, which is higher than the theoretical 8.4 Li⁺ reaction. The additional 1.1 Li⁺ could be attributed to the formation of the solid electrolyte interphase (SEI) layer on the surface of the material. The first charge capacity of GeO₂-nano shows higher capacity compared to the theoretical 4.4 Li⁺ reaction of GeO₂ (1127 mAh/g). This is due to the re-oxidation of germanium to form germanium oxides, which will be further discussed below. In the subsequent cycling at the 1 C-rate, the GeO₂-nano sample presents stable capacity of 1180 mAh/g up to the 7th cycle, and then the capacity fades gradually to 450 mAh/g after 50 cycles. The capacity fading can also be related to the sharp drop in the coulombic efficiency after the 7th cycle (Figure S4a). The capacity fading and the drop in coulombic efficiency can be related to the pulverisation of the electrode material where more active materials lose contact with the current collector after repeated cycling due to the volume expansion. In addition, the effects of the carbon coating on the electrochemical performance of GeO₂ can be seen from the GeO₂/C sample. The first discharge and charge capacities at the 0.05 C-rate are 2682 mAh/g and 2000 mAh/g, respectively, which correspond to 75% coulombic efficiency. The first cycle charge capacity of GeO₂/C is comparable to the GeO₂ theoretical capacity of 2152 mAh/g (8.4 Li⁺),

considering that the specific capacity calculated includes the carbon component in the sample, which is 11 wt%. Therefore, carbon-coating improves the coulombic efficiency by 20%, and it also enhances the reversibility of germanium re-oxidation during charging. Although the capacity and coulombic efficiency were increased tremendously, initial capacity fading from the 2nd to the 12th cycle is observed for the GeO₂/C sample cycled at the 1 C-rate. The capacity drops from 1865 mAh/g to 1400 mAh/g, and then the capacity is stable afterwards at 1400 mAh/g up to the 50th cycle. The coulombic efficiency of GeO₂/C also follows a similar pattern, where a drop in efficiency was observed up to the 12th cycle, and then the efficiency improved and stabilized to 99% up to the 50th cycle (Figure S4a). As for the GeO₂/Ge/C sample, the first discharge and charge capacity recorded is 2293 mAh/g and 1872 mAh/g, respectively, and the coulombic efficiency is 82%. The higher coulombic efficiency of GeO₂/Ge/C compared to GeO₂/C can be explained by the lower BET surface area and lower GeO₂ ratio. For charge at the 1 C-rate, 1770 mAh/g was recorded at the 2nd cycle, and a slight increase in capacity is observed up to the 30th cycle (1860 mAh/g). Then, slight capacity fading is observed and the capacity recorded at the 50th cycle is 1650 mAh/g. The extra capacity recorded for the GeO₂/Ge/C sample (theoretical capacity = 2152*0.64 + 1623*0.13 = 1588 mAh/g) can be due to: 1) lithium storage in the disordered carbon shells; 2) interfacial storage of Li-ions; 3) pseudo capacitance of Li-ions. The coulombic efficiency of GeO₂/Ge/C at the 2nd cycle is 99%, however, the efficiency gradually fades to 96% over 50 cycles. This trend is consistent with the gradual capacity fading of the GeO₂/Ge/C during cycling at 1 C-rate.

The lithium storage mechanisms of all the samples were investigated using cyclic voltammetry (CV), and the profiles are plotted in Figure 5. Three CV cycles were tested for each sample at the scan rate of 0.1 mV/s. In the first reduction scan of the GeO₂/Ge/C sample (Figure 5a), a

shoulder at about 1.3 V could be related to the formation of a vitreous phase lithium germanate and subsequent formation of amorphous Li_xGeO_2 .²⁶ The peak at 1.1 V is most probably due to formation of the SEI layer, as it is not reversible. In the voltage region between 0.75 V and 0.01 V, the peaks can be related to the lithium reactions with GeO_2 , which are described by the conversion reaction (Equation 1) and the alloying reaction (Equation 2). In the corresponding oxidation scan, the broad peak from 0.3 V to 0.7 V can be related to the de-alloying reaction, where lithium is removed from the Li-Ge alloy. Two broad humps at 1.1 V and 1.7 V can be related to the re-oxidation of germanium to germanium oxide. Although the re-oxidation of Ge to GeO_2 remains ambiguous, several metals and metalloids show similar peaks at these voltages, which correspond to the conversion reaction. Sandu *et al.* used Mossbauer spectroscopy to study the conversion mechanism of SnO_2 , and they found that the re-oxidation reaction occurs above 1.0 V.³⁶ More recently, Chen *et al.* showed evidence of a reversible conversion reaction of SnO_2 using ex-situ X-ray photoelectron spectroscopy (XPS) and TEM experiments.³² They too assigned the re-oxidation reaction to the voltage region above 1.0 V. Furthermore, direct evidence of the re-formation of Ge-O bonds in the charging cycle of a CuGeO_3 half-cell was observed using X-ray absorption near edge structure (XANES) and extended X-ray absorption fine structure (EXAFS) spectroscopy by Kim *et al.*²⁸ Based on these results, we propose that re-oxidation of Ge occurs during the oxidation scan (i.e. the charging cycle of the half-cell) in our $\text{GeO}_2/\text{Ge}/\text{C}$ sample. This is confirmed by ex-situ XPS at various depths of charge/discharge, as shown in Figure 6. It should be noted that the spectra shown in Figure 6 were analyzed after etching of about 90 nm of the surface using an ion gun in the XPS instrument. From the XPS spectrum of $\text{GeO}_2/\text{Ge}/\text{C}$ at discharge to 1 V, two obvious peaks indicated by the green (29.6 eV) and blue lines (32.4 eV) corresponds to the Ge-Ge and Ge-O bonds, respectively. After

discharging to 0.01 V, the peak indicating the Ge-O is not observed, which is due to the full conversion of GeO₂ to form Ge and Li₂O. In addition, the peak indicating Ge-Ge bonds has shifted to lower energy, which might be due to the formation of Li_xGe alloys. When the samples were charged to 2 V and 3 V, the Ge-O peak at 32.4 eV is observed which indicates the re-oxidation of germanium. Moreover, GeO₂/C (Figure 5b) also exhibit similar CV profiles to the GeO₂/Ge/C sample. The only variation is the decrease in reversibility of the conversion reaction component of the sample. This result is consistent with the cycling test in Figure 4a where capacity fading is observed in the first few cycles. Likewise, the GeO₂-nano and GeO₂-bulk samples show a small hump indicating the re-oxidation of germanium in the oxidation scans. This explains the higher capacity shown by the GeO₂-nano sample in the first cycle (Figure 4a; 1384 mAh/g compared to theoretically 1127 mAh/g for 4.4 Li⁺ reaction).

From the cycling performance curves, we found that the reversibility of the conversion reaction of GeO₂ is related to the carbon coating (GeO₂/C) and the introduction of metallic germanium (GeO₂/Ge/C) into the sample. In order to further understand this, the differential plots of all samples at the 15th cycle and the corresponding voltage profiles (the insets) are presented in Figure S5. Through investigation of the differential plots and the voltage profiles, it was found that the conversion reactions in GeO₂-nano and GeO₂-bulk were less reversible compared to the GeO₂/C and GeO₂/Ge/C samples. The small hump at 1.1 V in the charging cycle indicating re-oxidation of germanium was not observed after the 15th cycle in either the GeO₂-nano or the GeO₂-bulk samples. As for the GeO₂/C sample, the 1.1 V hump is still visible, however, the voltage profile at the 15th cycle shows that the plateau at 1.1 V has been significantly reduced. These results are consistent with the cycling performance. Thus, the observed capacity fading can be related to the decrease in reversibility of the conversion

reaction. The alloying reaction, on the other hand, shows good reversibility for both the GeO₂/C and the GeO₂-nano samples. In the case of the GeO₂/Ge/C sample, both the alloying and the conversion reaction with lithium are highly reversible. The charging curve of the 15th cycle shows an almost identical profile to that of the 1st charging cycle. From these results, we can conclude that nanosize particles are very important to enable the reversible conversion reaction. This is because nanoparticles have a larger surface area, which promotes the reaction kinetics. In addition, nanoparticles are known to show a smaller absolute volume change, which could keep the Li₂O and Ge in close proximity for the decomposition of lithia and simultaneous oxidation of germanium.³⁷ Furthermore, the carbon coating is an important factor in increasing the reversibility of the conversion reaction. As carbon is highly conductive, the interconnected carbon shells of the GeO₂/C and GeO₂/Ge/C samples would provide an efficient network for electron transfer, which in turn increases the kinetics of the lithium reactions. Moreover, the carbon shells could act as a buffer matrix to limit the volume variation during charge and discharge cycles.³⁸ Another important factor that we found in this work is the catalytic effect of germanium in the decomposition of Li₂O. Kim *et al.* reported the catalytic effect of copper in promoting the decomposition of Li₂O and facilitating the oxidation of germanium in CuGeO₃.²⁸ The germanium in the GeO₂/Ge/C sample plays a similar role to that of the Cu in the CuGeO₃. This can be seen from the excellent reversibility of the conversion reaction, even after 50 cycles at high rates. In addition, a schematic representation of the lithium reaction with GeO₂-nano, GeO₂/C and GeO₂/Ge/C which summarises the above points is presented in Figure 7.

Rate capabilities of the cells up to the 10 C-rate (21 A/g = 10.5 mA/cm²) were also tested, and the results are plotted in Figure 4c. The rate capability of the anode material is very important especially for the applications in electric vehicles.^{39,40} The GeO₂-nano sample showed good rate

capability, with charging capacity of 965 mAh/g, 915 mAh/g, 842 mAh/g, and 775 mAh/g recorded at the 1 C-rate, 2 C-rate, 5 C-rate, and 10 C-rate, respectively. When the rate was reduced to 0.1 C, the capacity recorded was only 870 mAh/g compared to the 1400 mAh/g recorded for the initial 0.1 C-rate cycles. This is consistent with the cycling results, where capacity fading was observed. As for the GeO₂/C sample, the capacity recorded at the 1 C-rate, 2 C-rate, 5 C-rate, and 10 C-rate was 1300 mAh/g, 1250 mAh/g, 1200 mAh/g, and 1050 mAh/g, respectively. The capacity was also recovered when the rate was reduced to 0.1 C (1350 mAh/g) again. The GeO₂/Ge/C sample shows the best rate capability among all the samples. At the 0.1 C-rate, the capacity recorded was 1850 mAh/g and the capacity recorded at the 0.5 C-rate was 1800 mAh/g. When the charging rates were increased to 1 C, 2 C, and 5 C, negligible capacity fading was observed, and the capacity recorded at the 5 C-rate was 1750 mAh/g. As the rate was further increased to 10 C, only a slight decrease in capacity was observed, and the capacity recorded was 1680 mAh/g. When the rate was reduced to 0.1 C, the capacity was fully recovered to 1850 mAh/g. The capacity at the 10 C-rate only shows a 10% decrease from the capacity recorded for the 0.1 C-rate cycles. The corresponding voltage profiles of the GeO₂/Ge/C sample at different rates are presented in Figure 4d. It should be noted that as the rate increases, only a slight increase in polarization was observed. The excellent rate capability of the GeO₂/Ge/C sample is due to several factors. Firstly, the nanosize nature of the individual particles provides higher surface area and shorter pathways for the lithium reactions. Secondly, the interconnected carbon shells, which form large clusters of up to 30 micrometers in size, provide a network of electronic pathways, which could increase the kinetics of lithium reactions. In addition, the unique nanostructure keeps the germanium and lithium oxides in close proximity after the discharge cycles, and therefore, it enhances the kinetics of the oxidation of germanium. From the

Raman spectra of both GeO₂/Ge/C and GeO₂/C samples (see SI; FigureS6), the I_D/I_G were determined to be 1 and 0.95, respectively. This indicates that both are disordered carbon and, therefore its effect on the electrochemical performance would not be significantly different due to the similarity of the I_D/I_G.

In conclusion, partial reduction of GeO₂/C led to the formation of Ge/GeO₂/C nanocomposite and demonstrated high capacity and good rate capability up to 10C rate. Such results were due to the reversible conversion reaction of the GeO₂ component by Ge catalytic effect. We found that the nanosized particles, carbon coating, and the elemental germanium in the composite play a crucial role in activating and improving the kinetics of the conversion reaction.

Supporting Information.

Experimental methods; BET analysis; SEM images; battery cycling data; differential plots; Raman spectroscopy; Fourier transform infra-red spectroscopy; this material is available free of charge via the Internet at <http://pubs.acs.org>.

Corresponding Author

zguo@uow.edu.au (Z. Guo); jpcho@unist.ac.kr (J. Cho)

Author Contributions

[§] These authors contributed equally.

Acknowledgement

This work is supported by an Australian Research Council (ARC) Discovery Project (Grant Number DP1094261) and National Research Foundation of Korea (NRF) grant funded by the

Korea Government (MEST) (No. 2012K001291). The authors would like to thank Dr. Tania Silver for critical reading of the manuscript and valuable remarks.

References

1. Chan, C. K.; Peng, H.; Liu, G.; McIlwrath, K.; Zhang, X. F.; Huggins, R. A.; Cui, Y. *Nature Nanotechnology* **2008**, 3, (1), 31-35.
2. Kim, H.; Han, B.; Choo, J.; Cho, J. *Angewandte Chemie-International Edition* **2008**, 47, (52), 10151-10154.
3. Liu, N.; Wu, H.; McDowell, M. T.; Yao, Y.; Wang, C.; Cui, Y. *Nano Letters* **2012**, 12, (6), 3315-3321.
4. Magasinski, A.; Dixon, P.; Hertzberg, B.; Kvit, A.; Ayala, J.; Yushin, G. *Nature Materials* **2010**, 9, (4), 353-358.
5. Ng, S.-H.; Wang, J.; Wexler, D.; Konstantinov, K.; Guo, Z.-P.; Liu, H.-K. *Angewandte Chemie-International Edition* **2006**, 45, (41), 6896-6899.
6. Wu, H.; Chan, G.; Choi, J. W.; Ryu, I.; Yao, Y.; McDowell, M. T.; Lee, S. W.; Jackson, A.; Yang, Y.; Hu, L.; Cui, Y. *Nature Nanotechnology* **2012**, 7, (5), 309-314.
7. Park, M.-H.; Kim, K.; Kim, J.; Cho, J. *Advanced Materials* **2010**, 22, (3), 415-+.
8. Park, M.-H.; Cho, Y.; Kim, K.; Kim, J.; Liu, M.; Cho, J. *Angewandte Chemie-International Edition* **2011**, 50, (41), 9647-9650.
9. Chan, C. K.; Zhang, X. F.; Cui, Y. *Nano Letters* **2008**, 8, (1), 307-309.
10. Seo, M.-H.; Park, M.; Lee, K. T.; Kim, K.; Kim, J.; Cho, J. *Energy & Environmental Science* **2011**, 4, (2), 425-428.
11. Yang, L. C.; Gao, Q. S.; Li, L.; Tang, Y.; Wu, Y. P. *Electrochemistry Communications* **2010**, 12, (3), 418-421.
12. Liu, X. H.; Huang, S.; Picraux, S. T.; Li, J.; Zhu, T.; Huang, J. Y. *Nano Letters* **2011**, 11, (9), 3991-3997.

13. Seng, K. H.; Park, M.-H.; Guo, Z. P.; Liu, H. K.; Cho, J. *Angewandte Chemie-International Edition* **2012**, 51, (23), 5657-5661.
14. Yu, Y.; Gu, L.; Wang, C.; Dhanabalan, A.; van Aken, P. A.; Maier, J. *Angewandte Chemie-International Edition* **2009**, 48, (35), 6485-6489.
15. Deng, D.; Kim, M. G.; Lee, J. Y.; Cho, J. *Energy & Environmental Science* **2009**, 2, (8), 818-837.
16. Hassoun, J.; Derrien, G.; Panero, S.; Scrosati, B. *Advanced Materials* **2008**, 20, (16), 3169-3175.
17. Deng, D.; Lee, J. Y. *Angewandte Chemie-International Edition* **2009**, 48, (9), 1660-1663.
18. Zou, Y.; Wang, Y. *Acs Nano* **2011**, 5, (10), 8108-8114.
19. Yu, Y.; Gu, L.; Zhu, C.; van Aken, P. A.; Maier, J. *Journal of the American Chemical Society* **2009**, 131, (44), 15984-+.
20. Lee, J.-I.; Lee, K. T.; Cho, J.; Kim, J.; Choi, N.-S.; Park, S. *Angewandte Chemie-International Edition* **2012**, 51, (11), 2767-2771.
21. Yoo, H.; Lee, J.-I.; Kim, H.; Lee, J.-P.; Cho, J.; Park, S. *Nano Letters* **2011**, 11, (10), 4324-4328.
22. Jeong, G.; Kim, J.-H.; Kim, Y.-U.; Kim, Y.-J. *Journal of Materials Chemistry* **2012**, 22, (16), 7999-8004.
23. Komaba, S.; Shimomura, K.; Yabuuchi, N.; Ozeki, T.; Yui, H.; Konno, K. *Journal of Physical Chemistry C* **2011**, 115, (27), 13487-13495.
24. Wang, X.-L.; Han, W.-Q.; Chen, H.; Bai, J.; Tyson, T. A.; Yu, X.-Q.; Wang, X.-J.; Yang, X.-Q. *Journal of the American Chemical Society* **2011**, 133, (51), 20692-20695.

25. Kim, Y.; Hwang, H.; Lawler, K.; Martin, S. W.; Cho, J. *Electrochimica Acta* **2008**, 53, (15), 5058-5064.
26. Pena, J. S.; Sandu, I.; Joubert, O.; Pascual, F. S.; Arean, C. O.; Brousse, T. *Electrochemical and Solid State Letters* **2004**, 7, (9), A278-A281.
27. Feng, J. K.; Lai, M. O.; Lu, L. *Electrochimica Acta* **2012**, 62, 103-108.
28. Kim, C. H.; Jung, Y. S.; Lee, K. T.; Ku, J. H.; Oh, S. M. *Electrochimica Acta* **2009**, 54, (18), 4371-4377.
29. Ning, J.; Jiang, T.; Men, K.; Dai, Q.; Li, D.; Wei, Y.; Liu, B.; Chen, G.; Zou, B.; Zou, G. *Journal of Physical Chemistry C* **2009**, 113, (32), 14140-14144.
30. Sakaushi, K.; Oaki, Y.; Uchiyama, H.; Hosono, E.; Zhou, H.; Imai, H. *Small* **2010**, 6, (6), 776-781.
31. Park, M.-S.; Kang, Y.-M.; Wang, G.-X.; Dou, S.-X.; Liu, H.-K. *Advanced Functional Materials* **2008**, 18, (3), 455-461.
32. Chen, Z.; Zhou, M.; Cao, Y.; Ai, X.; Yang, H.; Liu, J. *Advanced Energy Materials* **2012**, 2, (1), 95-102.
33. Du, G.; Zhong, C.; Zhang, P.; Guo, Z.; Chen, Z.; Liu, H. *Electrochimica Acta* **2010**, 55, (7), 2582-2586.
34. Guo, Z. P.; Du, G. D.; Nuli, Y.; Hassan, M. F.; Liu, H. K. *Journal of Materials Chemistry* **2009**, 19, (20), 3253-3257.
35. Wu, J.; Han, L.; Wang, N.; Song, Y.; Chen, H.; Chen, H.; Hu, J. *Crystengcomm* **2011**, 13, (14), 4611-4616.
36. Sandu, I.; Brousse, T.; Santos-Pena, J.; Danot, M.; Schleich, D. M. *Ionics* **2002**, 8, (1-2), 27-35.

37. Poizot, P.; Laruelle, S.; Grugeon, S.; Dupont, L.; Tarascon, J. M. *Nature* **2000**, 407, (6803), 496-499.
38. Fu, L. J.; Liu, H.; Zhang, H. P.; Li, C.; Zhang, T.; Wu, Y. P.; Holze, R.; Wu, H. Q. *Electrochemistry Communications* **2006**, 8, (1), 1-4.
39. Qu, Q.; Fu, L.; Zhan, X.; Samuelis, D.; Maier, J.; Li, L.; Tian, S.; Li, Z.; Wu, Y. *Energy & Environmental Science* **2011**, 4, (10), 3985-3990.
40. Tang, W.; Liu, L.; Zhu, Y.; Sun, H.; Wu, Y.; Zhu, K. *Energy & Environmental Science* **2012**, 5, (5), 6909-6913.

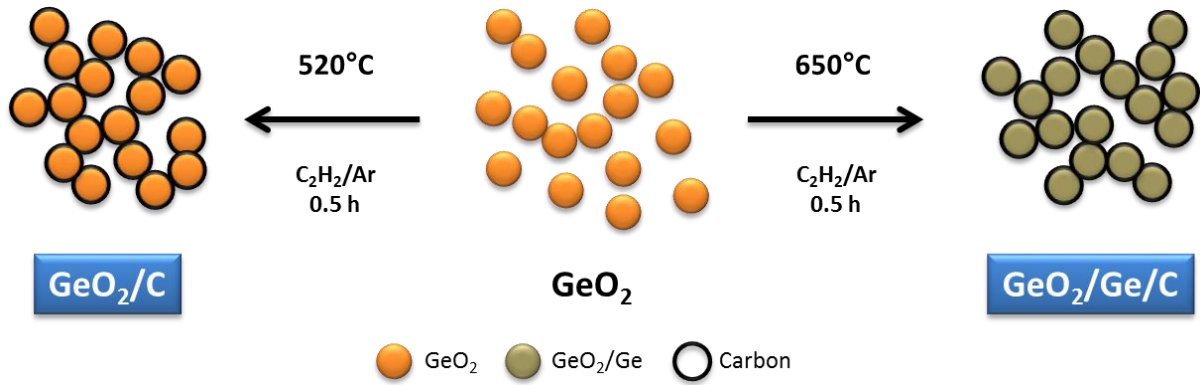


Figure 1. Schematic representation of the synthesis of GeO₂/Ge/C and GeO₂/C from GeO₂ precursor.

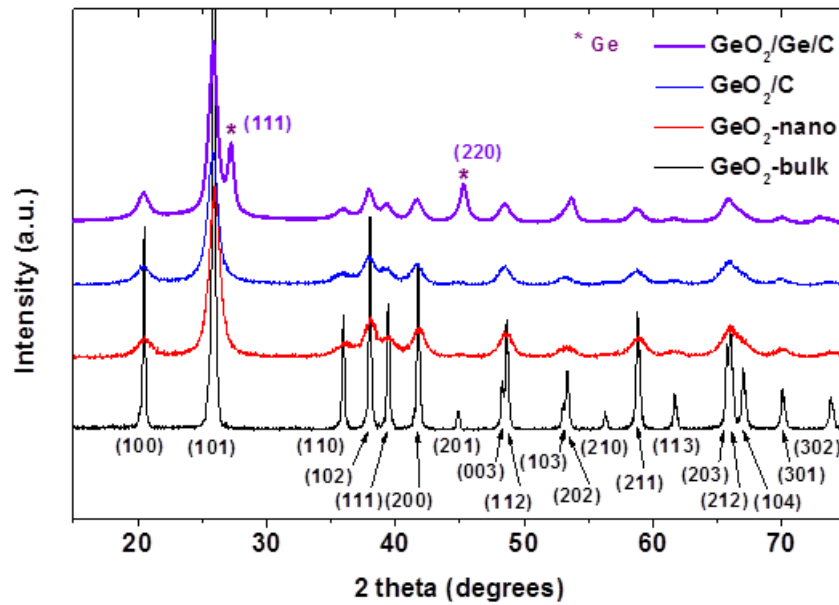


Figure 2. X-ray diffractions pattern of all the samples. The diffraction patterns of all GeO_2 samples matched hexagonal phase (ICDD# 36-1463) germanium dioxide, and the peaks are indexed. The peaks marked with asterisks, corresponds to diamond cubic germanium (ICDD#04-0545)

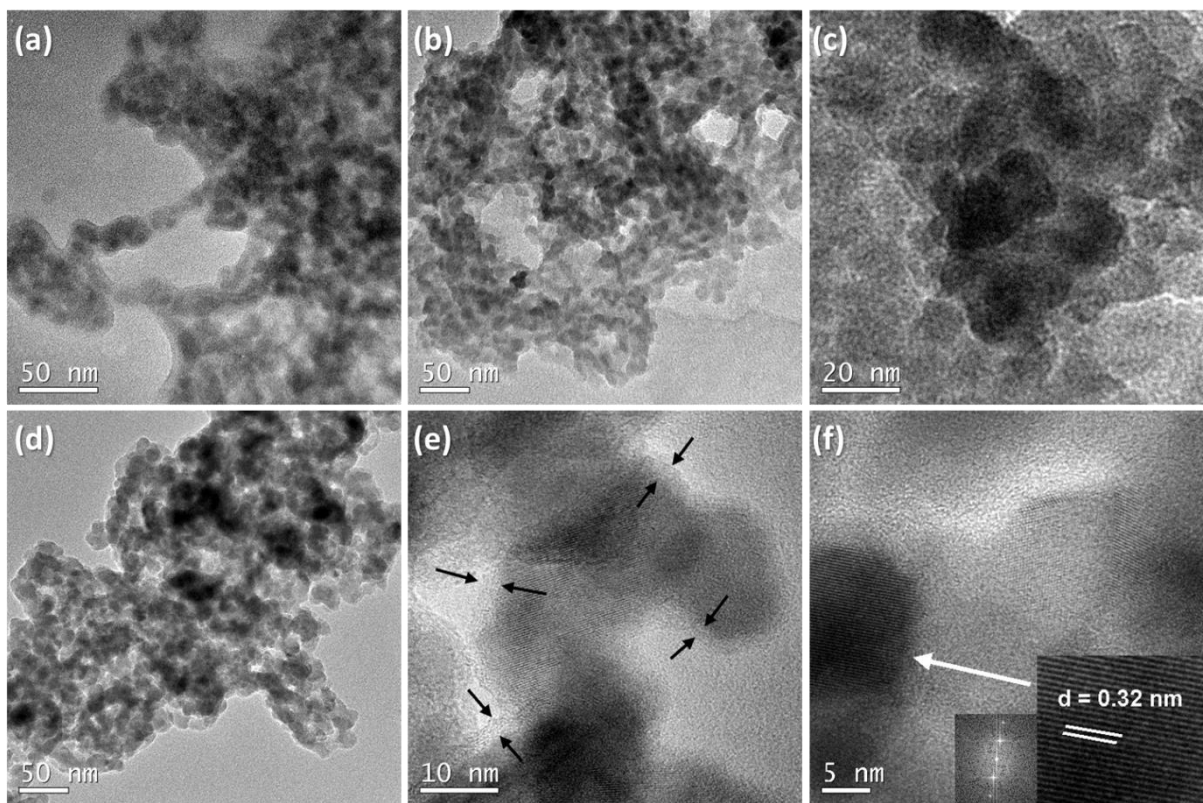


Figure 3. (a) Transmission electron microscope (TEM) image of GeO₂-nano with dense and light areas indicating amorphous regions of the sample. (b,c) TEM images of GeO₂/C sample showing similar particle size to the GeO₂-nano sample after carbon coating. The sample deforms under electron beam irradiation, and therefore, no lattice spacing could be observed. (d) TEM image of GeO₂/Ge/C sample showing similar morphology to the GeO₂/C sample. (e) HRTEM image of GeO₂/Ge/C. The black arrows show the carbon coating layers. (f) HRTEM image of GeO₂/Ge/C, the insets are an enlarged image of the area indicated by the white arrow (left) and the corresponding FFT pattern. The d-spacing of 0.32 nm corresponds to the (111) plane of germanium.

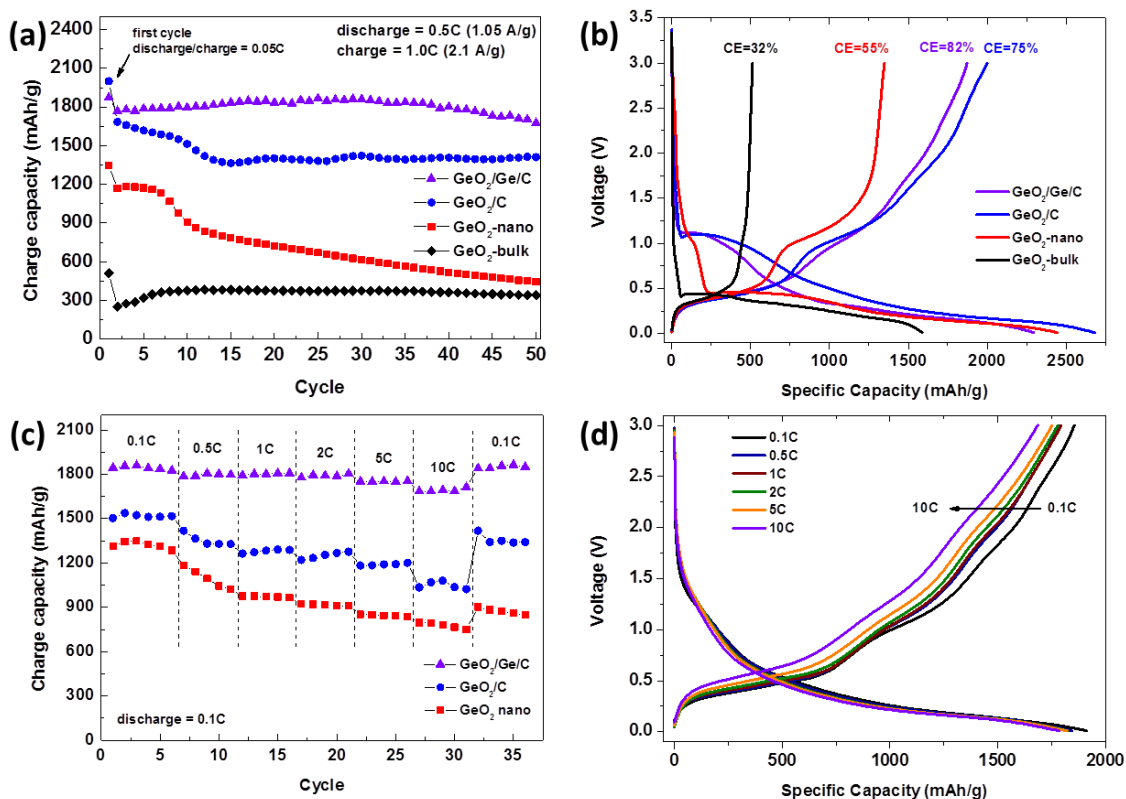


Figure 4. (a) Cycling performance of all the samples for 50 cycles at the 1 C-rate. The GeO₂/Ge/C sample shows excellent cycling performance, in which 90% of the capacity at the 2nd cycle was retained after 50 cycles. (b) Voltage profiles of all the samples at the first cycle at the 0.05 C-rate. GeO₂/Ge/C showed the highest coulombic efficiency (CE) of 82% followed by GeO₂/C (75%), GeO₂-nano (55%) and GeO₂-bulk (32%); (c) Rate performance of all the samples at the 0.1 C-rate, 0.5 C-rate, 1 C-rate, 2 C-rate, 5 C-rate, and 10 C-rate. The GeO₂/Ge/C sample showed the best rate performance, and the capacity at the 10 C-rate was 1680 mAh/g. (d) Voltage profiles of the GeO₂/Ge/C sample at various rates. Only a slight increase in polarization was observed when the rate was increased to the 10 C-rate.

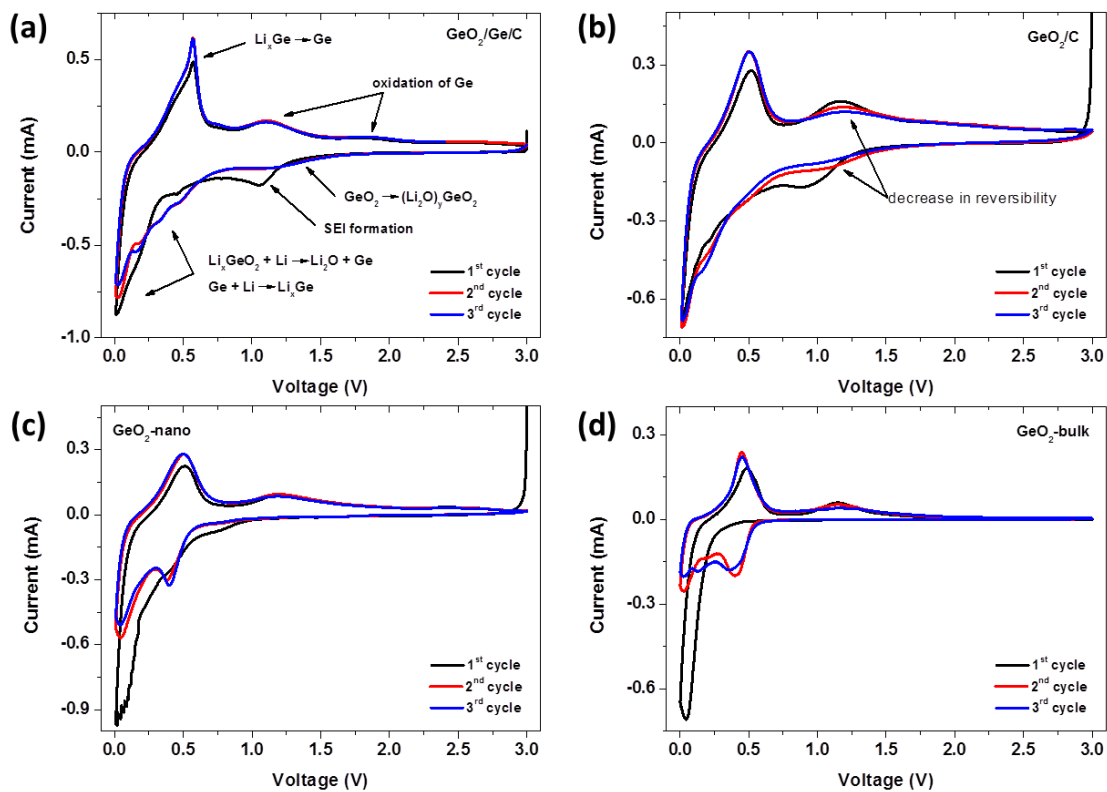


Figure 5. Cyclic voltammetry profiles of (a) $\text{GeO}_2/\text{Ge}/\text{C}$, (b) GeO_2/C , (c) $\text{GeO}_2\text{-nano}$ and (d) $\text{GeO}_2\text{-bulk}$ at the scan rate of 0.1 mV/s for 3 cycles.

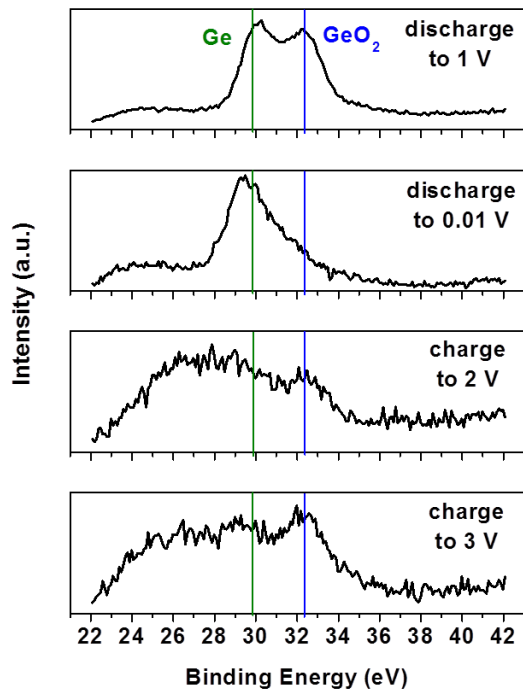


Figure 6. Ex-situ X-ray photoelectron spectroscopy analysis of the GeO₂/Ge/C sample at various depths of charge/discharge. At discharge to 1 V, the spectrum shows peaks indicating both Ge (green line) and GeO₂ (blue line). After discharging to 0.01 V, the peak indicating GeO₂ disappears. At charging to 2 V, the GeO₂ peak re-appears indicating oxidation of germanium. At 3 V, the GeO₂ peak becomes stronger.

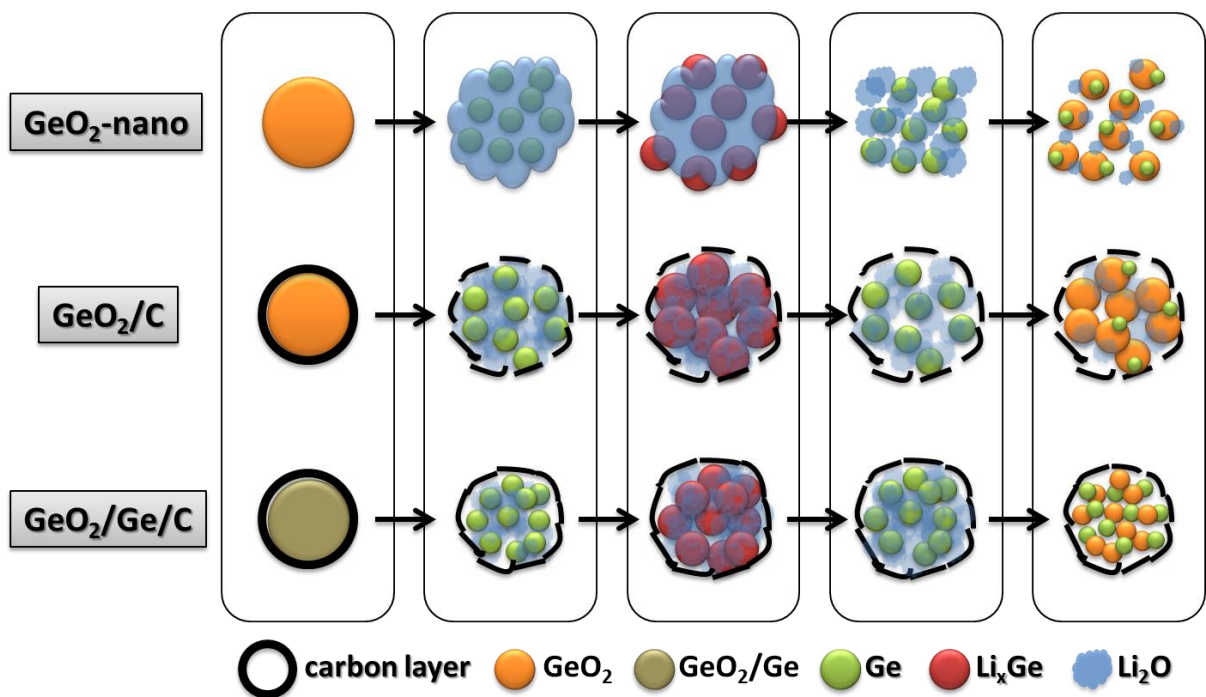


Figure 7. Schematic representation of the lithium reaction mechanism in all the samples. A reversible conversion mechanism of GeO₂ can be observed for GeO₂-nano, GeO₂/C, and GeO₂/Ge/C. The nano-sized GeO₂ particles are crucial for enabling the conversion reaction, while the carbon coating can improve the reversibility. The elemental germanium in GeO₂/Ge/C plays a crucial role as a catalyst in improving the reversibility of the conversion reaction of GeO₂.